Geophysical Journal International

Geophys. J. Int. (2012) **188,** 115–122 doi: 10.1111/j.1365-246X.2011.05266.x

Mapping deeply-buried geothermal faults using microtremor array analysis

Peifen Xu,[1] Suqun Ling,[2] Chuanjin Li,[1] Jianguo Du,[3] Dengming Zhang,[3] Xueqiu Xu,[3] Kangming Dai[4] and Zuohong Zhang[4]

[1] *Key Laboratory of the Study of Earth's Deep Interior, Institute of Geology and Geophysics, Chinese Academy of Sciences, Beijing* 100029, *China. E-mail: pfxu@mail.iggcas.ac.cn*
[2] *Geo-Analysis Institute Co. Ltd., Tokyo* 184-0012, *Japan*
[3] *Geological Survey of Jiangsu Province, Nanjing, Jiangsu* 210049, *China*
[4] *Geological Exploration Technology Institute of Jiangsu Province, Nanjing, Jiangsu* 210008, *China*

Accepted 2011 October 14. Received 2011 September 8; in original form 2011 March 19

SUMMARY

In this paper, the spatial autocorrelation microtremor array analysis is utilized to map deeply-buried subtle faults that have primary controls on geothermal reservoirs. We identified a low-velocity anomaly which is approximately 50 m wide at about 550–1400 m deep. A well drilled based on this anomaly later successfully produced hot water and further proved that the low-velocity anomaly was caused by a highly fractured zone at depths from 700 to 1500 m. Our results clearly demonstrate that the microtremor survey method can be effectively utilized to map deeply-buried faults and structures for geothermal energy exploration. The most effective way to increase the drilling success rate and, hence reduce the geothermal exploration risk, seems to be the development of new exploration methods and the integration of various geophysical technologies.

Key words: Time series analysis; Hydrogeophysics; Hydrothermal systems; Fractures and faults; Asia.

1 INTRODUCTION

Our earth's interior—like the sun—is a huge nuclear reactor, which provides almost never-ending heat energy from nature. This heat—geothermal energy—yields warmth and power that can be used in our daily life without polluting our environment. As a clean (no CO_2 emission), sustainable, flexible and reliable source of energy, geothermal energy has become increasingly attractive. Hot water from geothermal reservoirs at depth is the main target for development. Currently it is widely used for electricity generation and home heating, as well as providing energy for industrial and agricultural use. However, geothermal reservoirs are usually controlled by tectonic structures, leading to their heterogeneous distributions (Wang & Sun 2001). The amount of heat stored in a particular geothermal reservoir is often associated with the size and location of the geological structure. Geothermal reservoirs are difficult to detect or map because of their complex, diverse and relatively deep structures, For example, the southern region of Jiangsu Province in China is located in the area of the Sunan Uplift, a very complex geological structure. Geothermal reservoirs here have low to medium temperatures in the range of 25–90 °C. As hot water conduits and possibly storage, fractures and faults play a significant role in geothermal reservoir exploration and exploitation. Paleozoic sandstone, carbonate rocks and Mesozoic volcanic rocks in the province are the most common geothermal reservoir rocks. The exploration of geothermal resources to a large extent depends on the mapping of the fault systems that control the groundwater distribution.

Controlled Source Audio-frequency MagnetoTellurics (CSAMT) and the surface seismic reflection method are probably the most effective means to locate and map deep geological structures that control the distribution of geothermal reservoirs. However, in densely populated areas, these conventional methods often provide poor results primarily due to strong electromagnetic interferences, high human-related noises, and hence poor data quality. Therefore, there is a need to integrate various geophysical methods to reduce the associated risks and, hence, to improve the drilling success rate. This paper describes the Microtremor Survey Method (referred to as MSM) (Okada 2003, 2006) and its application to the mapping of deeply-buried fault structures for geothermal reservoir exploration.

2 THEORY AND METHOD

Microtremors are low-amplitude vibrations at the earth surface, which are usually caused by changes in weather, barometric pressure, ocean waves, tides, as well as human activities and noise produced by machineries in our daily life. The vibrations detected at the earth surface are typically composed of body waves (primary and secondary waves) and surface waves (Rayleigh and Love waves). It has been estimated that more than 70 per cent of the total energy

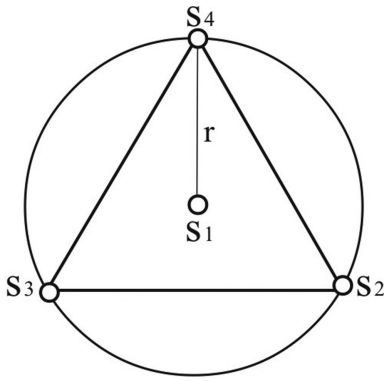

Figure 1. Illustration of the single-circle observation array for the SPAC method. Small circles on triangles represent microtremor station points.

in microtremors comes from the surface waves (Toksoz & Lacoss 1968). Although the waveform and the amplitude of these weak vibrations may vary with location and time, they are statistically stable over a certain period of time and space. Therefore, the stationary random process can be used to describe their behaviour (Aki 1957). Based on the principles of the stationary random process, MSM constructs the dispersion curve for the surface waves (the Rayleigh wave), from which it then inverts the shear-wave velocity structure.

The dispersion curve of the surface waves can be extracted from the vertical component of microtremors using the spatial autocorrelation (SPAC) method (Aki 1957; Ling 1994; Okada 2006). The spatial cross-correlation coefficient as a function of frequency for a given interstation distance, r, and angular frequency, ω, $\rho(r, \omega)$, averaged over many different azimuths, τ, can be written as

$$\rho(r,\omega) = \frac{1}{2\pi\varphi(r=0,\omega)} \int_0^{2\pi} \varphi(r,\theta,\omega)\,\mathrm{d}\theta = J_0\left(\frac{r\omega}{c}\right). \qquad (1)$$

where $\phi(r = 0, \omega)$ is the average autocorrelation function at the centre of the array, $\phi(r, \theta, \omega)$ is the cross-correlation function between the record at a site at coordinates (r, θ), and the record obtained at the station origin, c is the phase velocity at the site and J_0 is the Bessel function of first kind and order zero. The only unknown in the preceding equation is the phase velocity for each frequency, which can be obtained from the inversion of the observed correlation coefficients (e.g. Aki 1957; Ling 1994; Okada 2003, 2006).

The SPAC method requires a circular observation array that the microtremor sensors are stationed in a circle. Fig. 1 shows a typical circular observation array (a single-circular array) for the SPAC data acquisition. It is composed of four stations, one of them is placed at the centre (S1), the other three (S2–S4) are equally spaced on the circumference of a circle with radius r, forming an equilateral triangle. Here r is called the observation radius. To avoid confusion, we call the sensor location as the station point. Based on the numerical simulation results, the wavelength detected by the SPAC method can be more than 8.7 times of the observation radius (Miyakoshi *et al.* 1996). When surface waves approach the stations in three or more different directions, the SPAC method can detect wavelengths up to

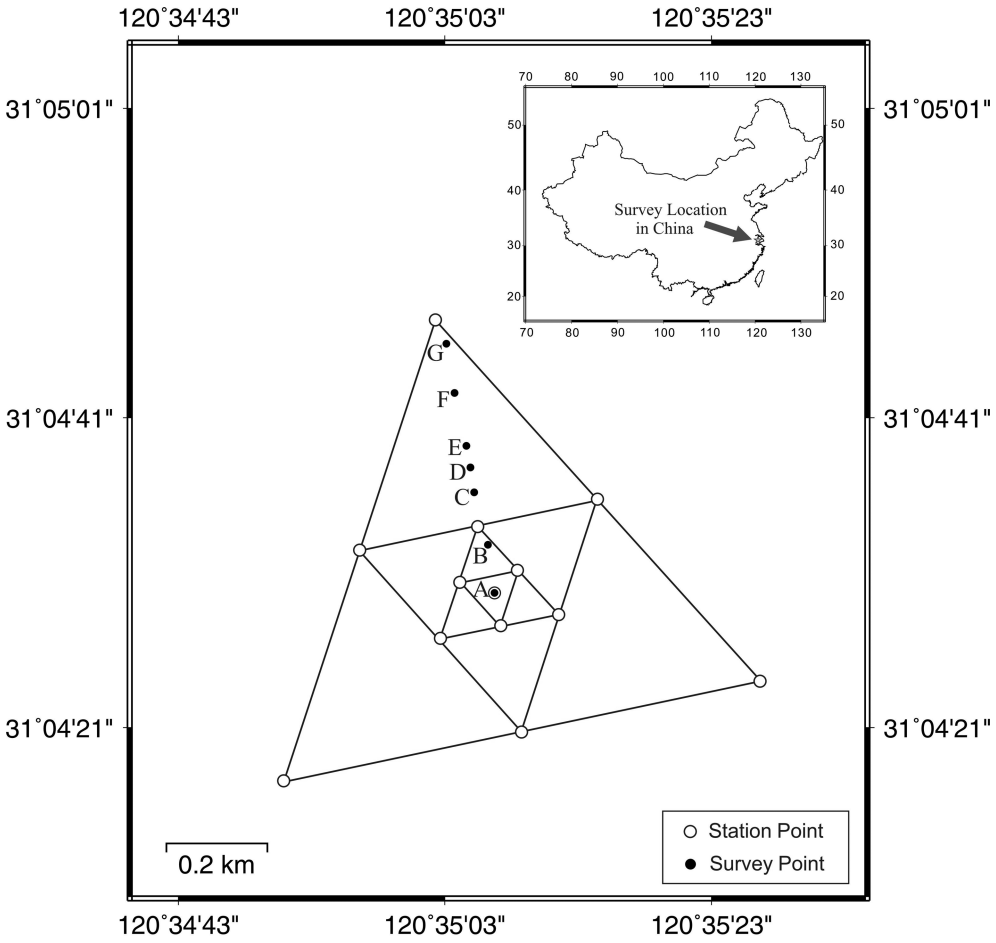

Figure 2. The survey location (upper right) and the layout (middle) of the microtremor observation site. Small open circles on triangles and its centre represent microtremor station points of survey point A. Similar observation layouts for the rest of the survey points are not shown here.

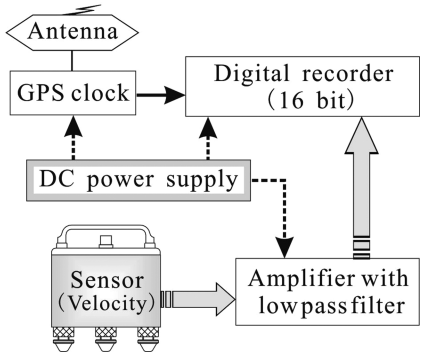

Figure 3. Block diagram of the observation equipment system. The sensors are of a velocity type with a natural frequency of 1 Hz, which is reduced to 0.2 Hz using the extension circuit.

10 times of the observation radius (Ling 1994). From observation data of actual microtremors, however, the detectable wavelength is often three to four times of the observation radius r by the SPAC method (Yamamoto 1998). Therefore, the detection depth of the observation array for the SPAC method depends on its radius. In general, the detection depth is about three to five times of the observation radius (Okada 2003). To have sufficient detection depth, actual observation arrays may consist of multiple circular arrays with different radii r. To obtain a 2-D section to show geologic structures (e.g. faults), the method described earlier will be carried out point-by-point along a pre-defined 2-D observation line. We call the point at which a microtremor survey is carried out as the survey point.

3 DATA ACQUISITION

Here we take a geothermal prospecting project carried out at Wujiang City, Southern Jiangsu, as an example to demonstrate how MSM works. The geothermal well is located in the coastal area of city's Tai Lake. A 2-D seismic section and a CSAMT section that acquired and processed before this work were integrated in the interpretation. A low-resistivity anomaly in the CSAMT data indicated a possible fractured zone filled with salty water. As shown in Fig. 2, a total of seven microtremor survey points (A–G) were arranged along a 2-D line. The spacings between the adjacent two points are: AB = 106.5 m, BC = 105 m, CD = 52.5 m, DE = 43.5 m, EF = 105 m, FG = 104 m. At each survey point, we used a multiple circular array with four observation circles. Their corresponding observation radii are 600, 300, 150, and 75 m, respectively. A total of 13 sensor stations are required for an observation system with four circular arrays (Fig. 2).

Fig. 3 shows the block diagram of the equipments needed at each station. We used single-component (vertical component) velocity-type sensors with a natural frequency of 1 Hz. However, the use of an extension circuit reduced the natural frequency to 0.2 Hz. This

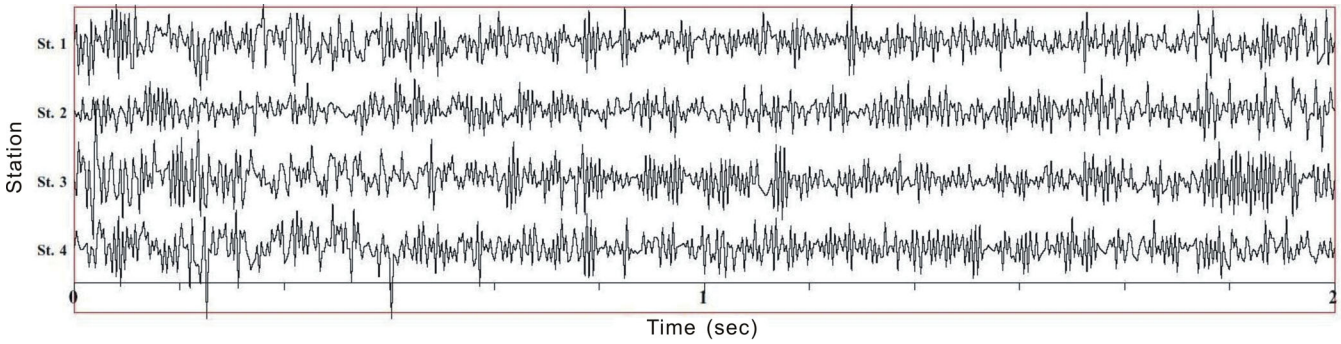

Figure 4. An example of the microtremor records at survey point B (array with circles observation radius 75 m). Each trace represents the vertical component of the surface particle motion at each sensor's location.

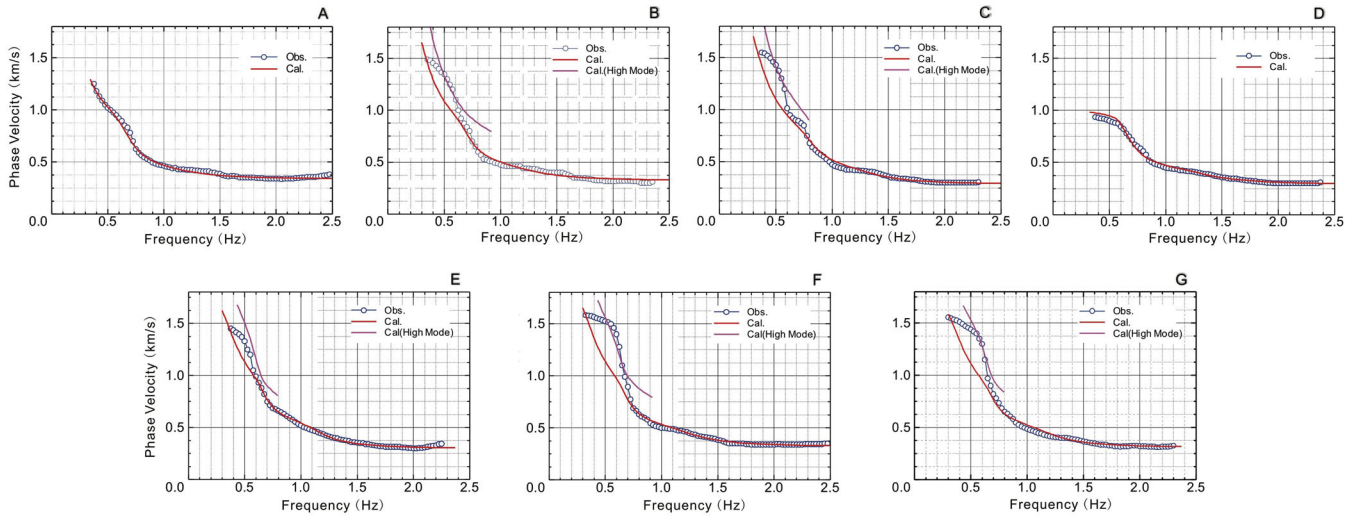

Figure 5. Calculated dispersion curves at the seven survey points.

is very important because lower natural frequency means deeper detection depth. A total of 30 min data were recorded simultaneously at the seven locations for each size of array using 16 bits digital recorders. The records were synchronized with the slow code generated by Global Positioning System (GPS) clocks. A sampling rate of 100 Hz and a low-pass filter with a high cut-off frequency of 10 Hz were adopted. Fig. 4 is an example of the recorded microseisms.

Consequently, we have obtained seven data sets from seven survey points. These data sets contained 30 min data. Because recorded data are occasionally contaminated by human-related noise, such as the vibration from vehicles, factories, and so on, we chose multiple good-quality portions from each data set for the analysis. The length of each portion was 40.96 s.

4 DATA PROCESSING AND RESULTS

We estimated Rayleigh-wave phase velocities from the vertical components using the SPAC method (Aki 1957). During the estimation we used the data at survey points A and D to calculate the phase velocity of Rayleigh-wave's fundamental mode. Data from the other five stations are also used to calculate the Rayleigh-wave phase velocity of the higher modes, in addition to its fundamental mode.

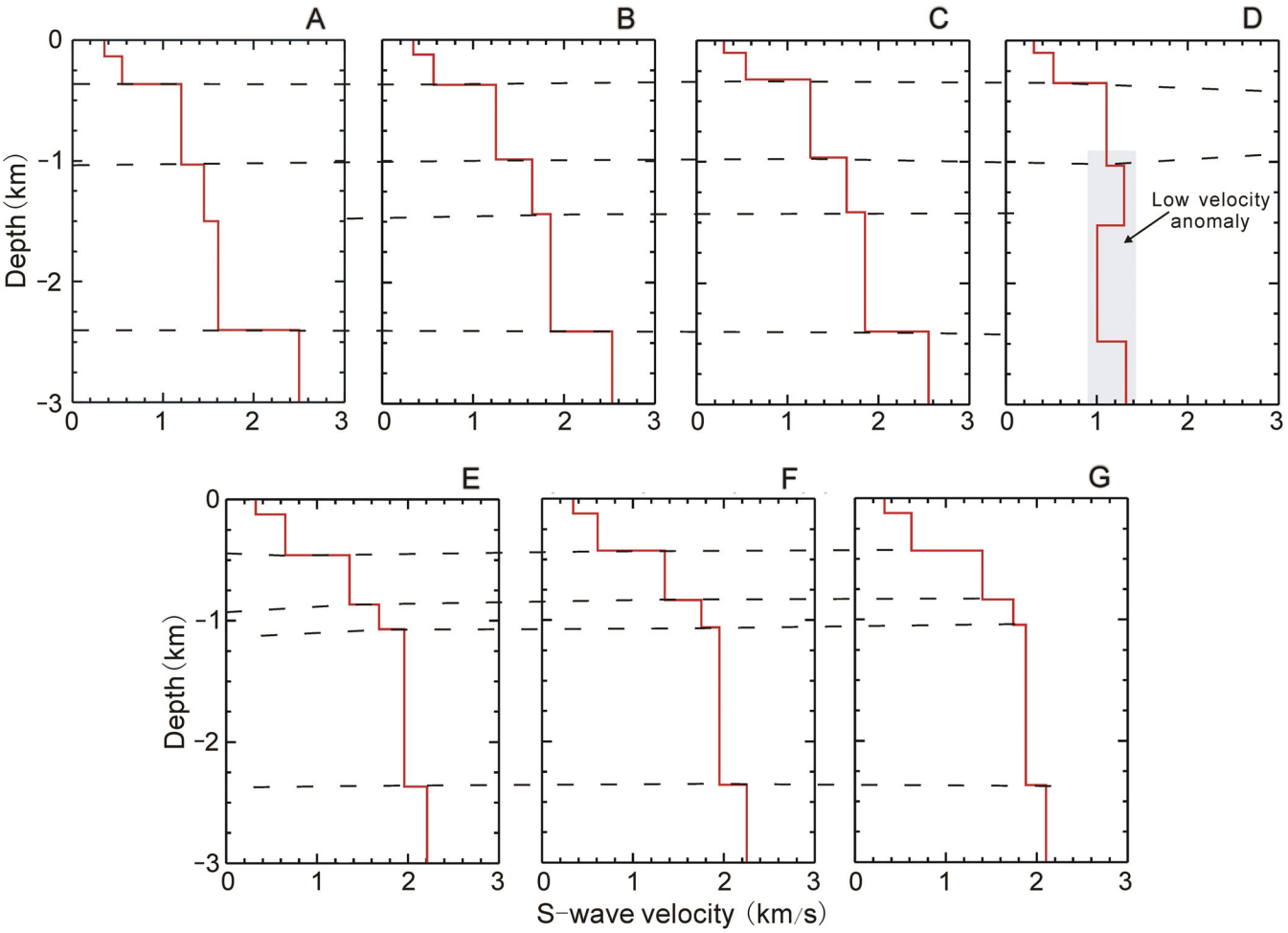

Figure 6. The inverted *S*-wave velocity structures. Note the low-velocity anomaly at survey point D.

Table 1. The inverted *S*-wave velocity model.

Survey Points													
A		B		C		D		E		F		G	
V_s	H	V_s	H	V_s	H	V_s	H	V_s	H	V_s	H	V_s	H
0.355	135	0.340	120	0.300	100	0.305	100	0.315	120	0.340	120	0.325	120
0.550	365	0.565	370	0.540	320	0.520	360	0.640	455	0.610	425	0.610	430
1.200	1030	1.250	985	1.250	965	1.105	1040	1.355	865	1.380	835	1.400	835
1.450	1500	1.650	1435	1.650	1415	1.300	1535	1.670	1070	1.750	1060	1.740	1045
1.610	2420	1.850	2405	1.850	2400	1.000	2490	1.950	2370	1.950	2360	1.880	2365
2.500	–	2.530	–	2.550	–	1.320	–	2.200	–	2.250	–	2.100	–

V_s, *S*-wave velocity (km/s); H, the depth of the layer's base (m).
Shaded numbers indicate the low-velocity layer.

Fig. 5 is the Rayleigh-wave phase velocities dispersion curve of each survey point.

A 1-D shear-wave velocity models down to a depth of about 3 km were estimated by fitting of the observed and the theoretical phase velocities through a non-linear inversion using a genetic algorithm (GA; Cho *et al.* 1999). The estimated shear-wave velocity model is shown in Fig. 6 and listed in Table 1.

The relative changes in *S*-wave velocity are usually good enough to visually show anomalous geological bodies, without knowing the absolute values of the inverted *S*-wave velocity values. The following equation is often used to convert the dispersion curve ($V_r \sim f$, V_r denotes the Rayleigh-wave phase velocity, f is frequency) to the apparent *S*-wave velocity profile ($V_x \sim H$, V_x is the apparent *S*-wave velocity, H represents depth; Ling & Miwa 2006), which gives clear image of lateral variations in rock properties

$$V_{xi} = \left(\frac{t_i v_{ri}^4 - t_{i-1} v_{r(i-1)}^4}{t_i - t_{i-1}} \right)^{1/4}, \tag{2}$$

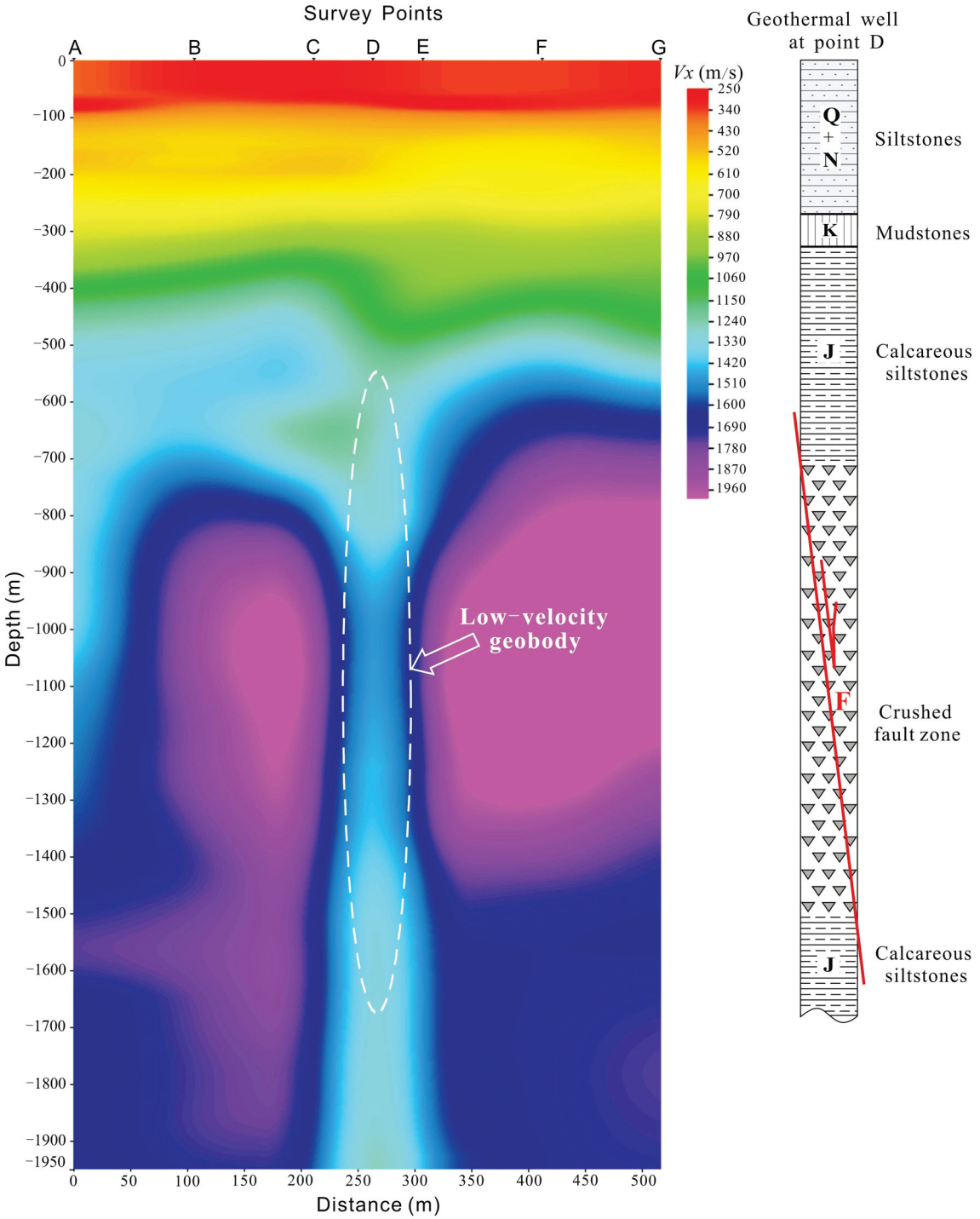

Figure 7. The microtremor V_x cross-section. The geologic column from a well drilled later at survey point D is displayed on the right for comparison. The fault/fracture related low velocity anomaly indicated by using white dashed line.

where t_i is the period. Subscript i denotes the ith point. V_x is the apparent S-wave velocity which has a dimension of velocity. A laterally continuous S-wave velocity profile can then be obtained through lateral data interpolation. The obtained final result will be used for interpreting the relative lateral changes in lithology and geological structures. Fig. 7 is the apparent S-wave velocity profile (V_x-profile).

Both Figs 6 and 7 show an anomalous low-velocity geobody (as indicated by the white dashed line in Fig. 7) underneath the survey point D. The shear-wave velocity at the shallow depths from 0 to 300 m behaves normal and laterally continuous. There is a weak velocity difference between the low-velocity geobody and its surrounding rock at depths from 300 to 700 m. However, the velocity difference becomes significantly bigger at depths from 700 to 1400 m. At its adjacent survey points C and E, the shear-velocity is on the normal trend. The estimated width for the low-velocity geobody is approximately 50 m, which increases slightly with depth downward. A 100 m wide low-resistivity geobody under D, extending from the surface to approximately 1500 m, was also observed from a CSAMT section. The low-velocity and low-resistivity anomaly was interpreted to be a result of a highly fractured (damaged) zone in the region, indicating an ideal location for drilling a geothermal well.

On the basis of the integrated MSM and CSAMT results, a geothermal well was drilled at location D, reaching a total depth of 1680 m. The drilling result revealed a layer of approximately 275 m of Cenozoic lacustrine deposit at the top. The Jurassic strata from 275 to 1680 m mainly consist of calcareous siltstones, volcanic breccia and tuff. The drilling result also showed a heavily fractured zone between 700 and 1500 m (showed in Fig. 7 right), which confirmed our interpretation. The well successfully produced 383 m^3/d of hot water with temperature of ∼46 °C, meeting our customer's design requirements.

5 DISCUSSION

We successfully applied MSM based on the SPAC method to determine well locations for geothermal reservoir exploration. A ∼50 m wide low-velocity anomaly below the Cenozoic lacustrine deposit at the survey point D is detected. We interpreted it as a result of a highly-fractured zone. Our interpretation was later confirmed by the new drilling results, indicating that the MSM is possibly the most effective way to detect and map fractured/faulted zones, limestone caverns, water-bearing strata and other geological features. Shear-wave velocity profiles from single-point MSM can be used to estimate geothermal reservoir's depth and thickness, providing critical information for drilling.

It is commonly believed that it is difficult or impossible to detect anomalous geobodies with sizes much smaller than the average seismic wavelength. Although this is theoretically true, the question is how small is detectable for a given seismic wavelength. In the oil and gas exploration, the detectable thickness can be as small as one tenth of the average wavelength. In fact, the minimum detectable size depends not only on the wavelength, but also on the velocity contrast. In this particular case, the dominant wavelength (roughly 1000 m) is approximately 20 times of the width (∼50 m) of the fractured zone. We believe that the following two factors contribute to the detectability of such small geophysical anomalies: (1) large velocity contrast between the fractured zone and its surrounding rock and (2) the unique characteristics of the method itself.

The first factor can be easily proved, since numerous published results demonstrated the high sensitivity of seismic velocity to the presence of fractures (e.g. Hudson 1981). However, a few sentences are needed here to explain the second factor. When a microtremor station is located above the low velocity zone, the violation of the layered-medium assumption due to strong lateral velocity change generally leads to the underestimate of the shear-wave velocity. Although the estimated shear-wave velocity does not represent the true geology (lower than the true shear-wave velocity), it otherwise enhances the low-velocity anomaly and therefore helps us to detect even smaller velocity anomalies.

The theoretical proof of the concept described above is extremely difficult, if possible. Here we simply provide another real example from the Eastern region of Jiangsu Province, PR China, to further demonstrate effectiveness of MSM for fractured-zone detection. In

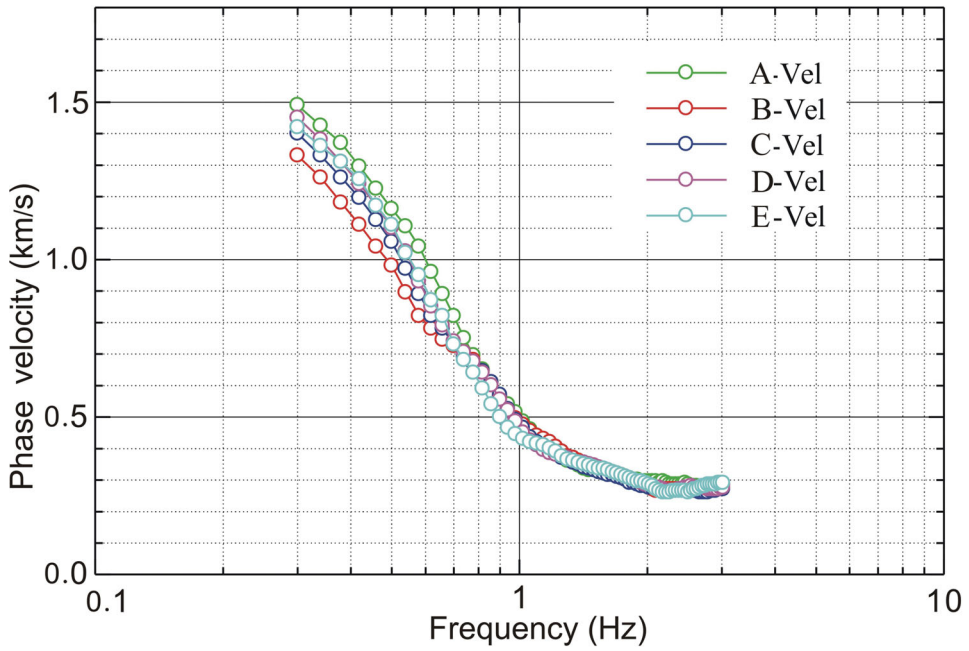

Figure 8. The shear-wave phase velocity dispersion curves observed from another microtremor survey with main result shown in Fig. 9.

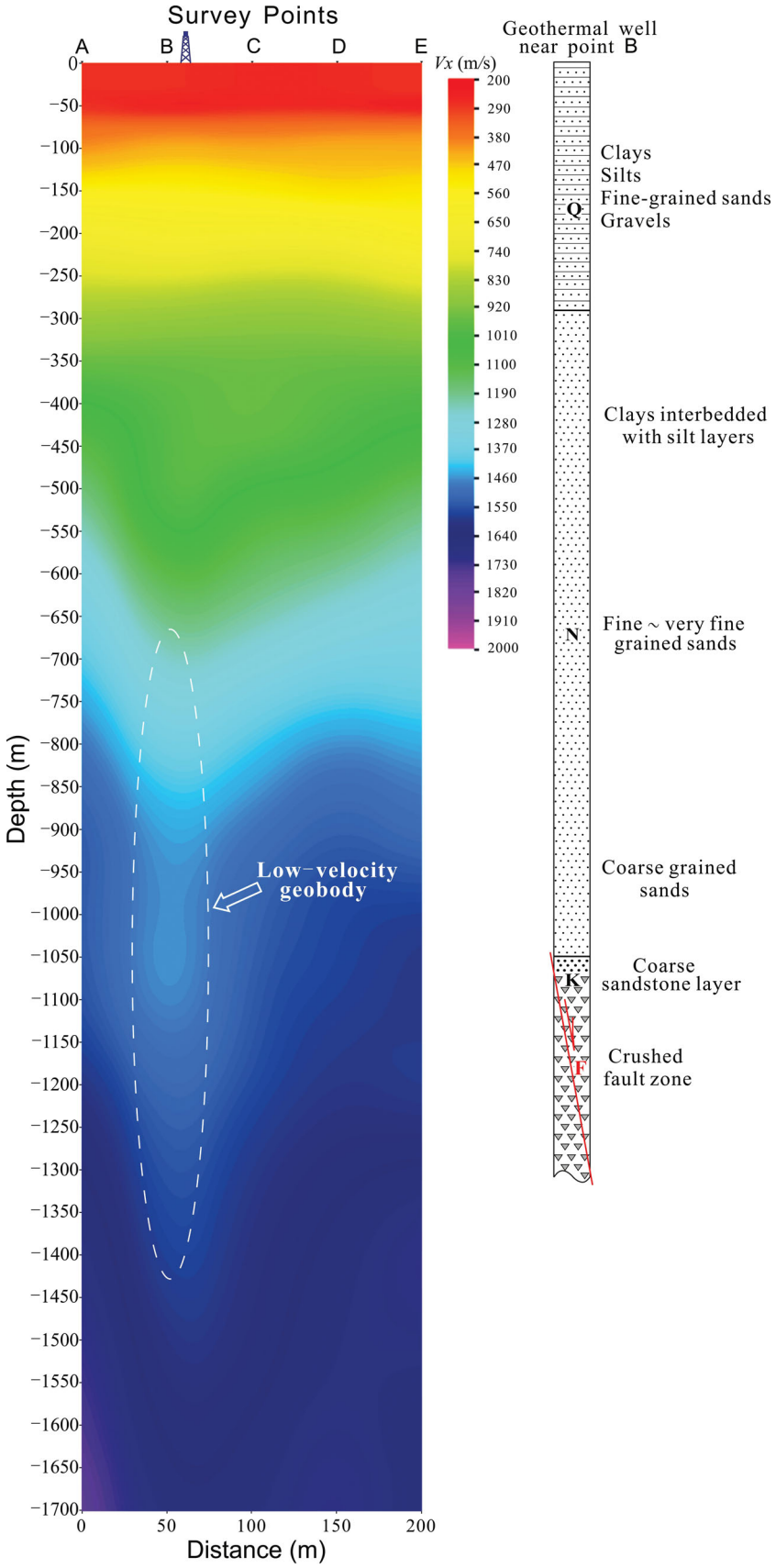

Figure 9. Inverted apparent *S*-wave velocity section using microtremor data acquired at a geothermal exploration site in the Eastern Jiangsu Province.

this example, we have 5 survey points A∼E. Their dispersion curves are shown in Fig. 8. The shear-wave phase velocities in the frequency range of 0.3 to 0.7 Hz at survey point B are obviously lower than those at other survey points. Fig. 9 shows the apparent shear-wave velocity section, inverted from the dispersion curves in Fig. 8 using the method described earlier. We observed a low-velocity anomaly from 500 m to as deep as 1300 m beneath the survey point B. Its velocity contrast with its surrounding rock reaches the maximum at depths around 1100 m. A well drilled based on our MSM result verified the interpretation. As shown in Fig. 9, the Quaternary sediments (above 290 m) mainly consist of clays, silts, fine-grained sands and gravels. The Tertiary Neogene formations start at 290 m with yellow clays interbedded with silt layers in the upper, followed by green fine to very fine grained sands in the middle and finish with coarse grained sands and occasionally gravels interbedded with clay layers on the bottom at ∼1050 m. The well penetrated a fracture zone just below a Cretaceous coarse sandstone layer at ∼1070 m. The well successfully produced more than 3000 m^3 of hot water (76 $^\circ$C) per day.

More successful fracture zone detection examples can also be found from Xu *et al.* (2009). MSM is applicable to gentle geological structures to obtain accurate *S*-wave velocity. At places where there are strong lateral changes in rock properties, such as heavily faulted, fractured, and damaged zones, the distorted dispersion curves will generate considerable errors in the inverted *S*-wave velocity. Even though its absolute values may not make sense, the lateral velocity changes can be used to identify anomalous geobodies, for example fractured zones.

However, geothermal reservoirs are often deeply-buried, controlled by complex geological structures, and hence difficult to detect using a single geophysical technique. It is necessary to integrate MSM with other conventional geophysical methods (e.g. CSAMT) to increase the drilling success rate.

ACKNOWLEDGMENTS

The authors are very grateful to two anonymous reviewers for their constructive comments and suggestions helped us to improve the manuscript. We are grateful to the Editor and Associate Editor for their critical review of this paper. The first author thank the Geothermal Center of Geological Survey and Geological Exploration Technology Institute of Jiangsu Province for their cooperation in providing the support and permission to publish this work. This research was financially supported by the Chinese Academy of Sciences (KZCX2-EW-107) and National Natural Science Foundation of China (Grants No. 40874025) to P. Xu.

REFERENCES

Aki, K., 1957. Space and time spectra of stationary stochastic waves, with special reference to microtremors, *Bull. Earthquake Res. Inst.,* **35,** 415–457.

Cho, I., Nakanishi, I. & Ling, S.Q., 1999. Application of Forking Genetic Algorithm fGA to an exploration method using microtremors, *BUTSURI-TANSA (Geophys. Explor.),* **52,** 227–246.

Hudson, J.A., 1981. Wave speeds and attenuation of elastic waves in material containing cracks, *Geophys. J. R. astr. Soc.,* **64,** 133–150.

Ling, S.Q., 1994. Research on the estimation of phase velocities of surface waves in microtremors, *PhD thesis*, Hokkaido University, Japan.

Ling, S.Q. & Miwa, S., 2006. The evaluation of soil structures by Surface Wave Prospecting Method and Microtremor Survey Method—2004 Mid Niigata Prefecture Earthquake, in *A New Technique on Engineering Geophysical Method,* pp. 80–85, ed. Liu, Y.Z., Geological Publishing House, Beijing.

Miyakoshi, K., Okada, H. & Ling, S.Q., 1996. A range of wavelengths possible to estimate phase velocities of surface waves in microtremors, *Proceedings of the 94th SEGJ Conference,* Tokyo, pp. 178–182.

Okada, H., 2003. *The Microtremor Survey Method*, Geophysical Monograph, Vol. 12, Society of Exploration Geophysicists, Tulsa, OK.

Okada, H., 2006. Theory of efficient array observations of microtremors with special reference to the SPAC method, *Explor. Geophys.,* **37,** 73–85.

Toksoz, M.N. & Lacoss, R.T., 1968. Microtremors—mode structure and sources, *Science,* **159,** 872–873.

Wang, J. & Sun, Z., 2001. *Amazing Geothermal,* Tsinghua University Press, Beijing.

Xu, P.F., Li, C.J., Ling, S.Q., Zhang, Y.B., Hou, C. & Sun, Y.J., 2009. Mapping collapsed columns in coal mines utilizing microtremor survey methods, *Chinese J. Geophys.,* **52,** 1923–1930.

Yamamoto, H., 1998. Analytical and experimental approaches to the method for estimation of phase velocities using the data of microtremors with three components, *PhD thesis*, Hokkaido University, Japan (in Japanese).